

1 **Formation of recurring transient Ca²⁺-based intercellular communities during**
2 ***Drosophila* hematopoiesis**

3 Saar Ben David^{1*}, Kevin Y.L. Ho^{2*}, Guy Tanentzapf^{2&}, Assaf Zaritsky^{1&}

4 ¹Department of Software and Information Systems Engineering, Ben-Gurion University of the
5 Negev, Beer-Sheva 84105, Israel

6 ²Department of Cellular and Physiological Sciences, University of British Columbia, Vancouver,
7 BC V6T 1Z3, Canada

8 *Equal contribution

9 &Co-corresponding authorship

10 Assaf Zaritsky, assafzar@gmail.com

11 Guy Tanentzapf, guy.tanentzapf@ubc.ca

12

13

14

15

16

17

18

19

20

21

22

23

24 **Abstract**

25 Tissue development occurs through a complex interplay between many individual cells. Yet, the
26 fundamental question of how collective tissue behavior emerges from heterogeneous and noisy
27 information processing and transfer at the single-cell level remains unknown. Here, we reveal that
28 tissue scale signaling regulation can arise from local gap-junction mediated cell-cell signaling
29 through the spatiotemporal establishment of an intermediate-scale of transient multicellular
30 communication communities over the course of tissue development. We demonstrated this
31 intermediate scale of emergent signaling using Ca^{2+} signaling in the intact, ex vivo cultured, live
32 developing *Drosophila* hematopoietic organ, the Lymph Gland (LG). Recurrent activation of these
33 transient signaling communities defined self-organized signaling “hotspots” that receive and
34 transmit information to facilitate repetitive interactions with non-hotspot neighbors, transfer
35 information across cells, and regulate the developmental progression of hotspots. Overall, this
36 work bridges the scales between single-cell and emergent group behavior providing key
37 mechanistic insight into how cells establish tissue-scale communication networks.

38

39 **Significance statement**

40 Cells coordinate their internal state and behavior by exchanging information with other cells in
41 their vicinity. These local interactions are integrated across space and time to enable
42 synchronized function at the tissue scale. Using live microscopy imaging of the *Drosophila*
43 Lymph Gland, and by applying computational analyses, we identified and characterized a new
44 mode of cellular communication through self-organized recurring coordinated short-term
45 activation at the intermediate scale of 3-8 cells, which we call “hotspots”. We reveal that
46 hotspots form over the course of tissue development, and are dependent on specific proteins,
47 called gap-junctions, that enable communication between adjacent cells. Hotspots repeatedly
48 transmit and retrieve information to and from their non-hotspot neighbors to spread information
49 throughout the tissue to regulate and coordinate tissue function.

50

51 Introduction

52 The emergence of collective cell behavior is an essential component of many basic biological
53 phenomena such as tissue morphogenesis (1), cell migration (2), or bacterial quorum sensing (3,
54 4). Key to understanding collective cell decision-making is elucidating how local information
55 transfer between cells is integrated in space and time. This spatial and temporal integration of
56 information is essential for regulating the emergence of collective behavior at the multicellular
57 scale (5, 6). The *Drosophila* hematopoietic organ, the Lymph Gland (LG), is a powerful,
58 genetically tractable, model to study how information is integrated in space and time to facilitate
59 collective cell behavior. The LG contains dozens of stem cell-like blood progenitors that are
60 largely quiescent but can be collectively activated in certain conditions, such as in response to
61 pathogenic infection, to rapidly produce hundreds of highly differentiated blood cells with
62 infection-fighting characteristics (7, 8). Long-term culture and live imaging of the intact LG
63 showed that Calcium (Ca^{2+}) signaling, which is transmitted between blood progenitor cells through
64 gap-junctions, mediated essential information transfer across large distances in the LG (9). Ca^{2+}
65 levels serve a key function in controlling blood progenitor fate as the activity of multiple pathways
66 that regulate progenitor behavior, including JAK/STAT and CaMKII signaling, is modulated by
67 the amount of Ca^{2+} in the cell at a specific time (9, 10). Gap junctions, intracellular channels that
68 directly link adjacent cells to allow them to exchange ions and other small molecules, can help
69 cells form signaling networks (9, 11, 12). In characterizing, at the population scale, the gap-
70 junctions based, Ca^{2+} -mediated, multicellular signaling network in the LG we observed
71 synchronized cell pairs that were located up to 38 cell diameters ($\sim 190 \mu\text{m}$) from one another.
72 Importantly, functional studies illustrated that the gap-junction mediated Ca^{2+} -signaling network
73 was required for proper regulation and function of the LG by coordinating fate decisions at the
74 population scale (9). A key question that emerged from our previous results was how the local
75 information transfer between adjacent cell pairs formed a global multicellular network.
76 Specifically, we wanted to characterize and understand the intermediate stages that allowed cell-
77 cell signaling exchanged between individual cells to become collective signaling.

78 Here we identified, using spatiotemporal analysis of Ca^{2+} -signaling in live intact LGs, the gradual
79 formation of communicating communities of 3-14 progenitor cells over the course of development,
80 through intercellular gap junction-mediated signaling. Recurrent signaling activity of these

81 communities formed hotspots of local information transmission highlighting heterogeneity in
82 intercellular information transfer as a potential contributor to collective decision making. Taken
83 together, our results explain how the exchange of information between individual cells in the
84 *Drosophila* LG becomes an emergent behavior involving multiple cells. This provides insight into
85 the bridging of the scales between single-cell and emergent group behavior.

86

87 **Results**

88 **Propagating intercellular Ca²⁺ signaling forms communicating communities in the** 89 ***Drosophila* lymph gland**

90 We investigated Ca²⁺ signaling in individual blood progenitors using live imaging of intact, *ex*
91 *vivo* cultured, LGs (Fig. 1A). By manual qualitative selection of adjacent blood progenitor pairs,
92 we previously showed that Ca²⁺ signals propagate between neighboring blood progenitor pairs and
93 this propagation is mediated by gap junctions (Video S1) (9). To systematically and quantitatively
94 characterize the patterns of signal synchronization across scales in-depth, we measured the
95 temporal correlation between Ca²⁺ signals in all blood progenitor pairs in the LG. This analysis
96 identified a negative correlation between the distance between blood progenitor pairs (termed *cell*
97 *pair distance*) and the level of coordination in their Ca²⁺ signals (termed *cell pair correlation*).
98 This means that, on average, closer blood progenitor pairs were more synchronized in terms of
99 Ca²⁺ signaling than distant pairs (Fig. 1B, Fig. S1A). These data identified a sub-population of
100 highly synchronized cell pairs, where cells were located within a distance of approximately 14 μm
101 from one another, about two cell diameters apart. Indeed, partitioning the data to close ($\leq 14 \mu\text{m}$)
102 versus far ($\geq 14 \mu\text{m}$) cell pairs showed that close pairs were more likely to be in a higher level of
103 synchronization (Fig. 1C, Fig. S1B). This subpopulation of highly synchronized close-cell pairs
104 highlighted the heterogeneity in cell-cell information transfer. However, it was still unclear how
105 this local cell-cell synchronization propagates from the scale of cell pairs to the multicellular scale.
106 To detect and quantify collective spatiotemporal signaling events, i.e., signaling events that
107 involve more than two cells, we applied a computational method known as the “Automatic
108 Recognition of Collective Signaling” (ARCOS) (13). ARCOS binarizes the single blood
109 progenitor Ca²⁺ signal, according to its magnitude, to “active” (Ca²⁺ peak) or “inactive”, followed
110 by spatiotemporal clustering of cells that are synchronously active (peaks ≤ 15 seconds apart) (13).
111 This analysis defines “collective signaling events” that we refer to as local transient *communities*
112 of blood progenitor signaling (Video S2). Every community consists of a minimum of three cells

113 that were active simultaneously or within a 15-second delay. Using ARCOS, we were able to
114 monitor the formation and disintegration of a community (Fig. 1D, Video S3): following an initial
115 Ca^{2+} spike, subsequent activation of adjacent blood progenitors, as marked by red dots connected
116 by a white arrow, initiated a 3-cell community (Fig. 1D, 0-7 seconds). The community gradually
117 grew, which was observed as Ca^{2+} activation in adjacent cells (Fig. 1D, red dots and white arrows,
118 11-23 seconds) and shrunk by deactivation of cells in the community (Fig. 1D, yellow arrowheads,
119 18-25 seconds). Throughout its evolution, this community involved 6 cells (Fig. 1D, marked by a
120 white dashed polygon, 25 seconds) with a maximum of 5 cells being active simultaneously (Fig.
121 1D, 16 seconds). Our analysis identified communities of local intercellular transfer of signaling
122 information involving 3-14 blood progenitors per community, with a median community size of 4
123 cells and 30% of communities having at least 5 participating cells (Fig. S2, example in Video S3).
124 Two potential confounders of this analysis were the stochastic co-incidence of activation events
125 and the presence of areas with higher local cell densities, both of which may lead to the detection
126 of spurious collective signaling events by ARCOS (Fig. S3). To mitigate these potentially
127 confounding factors, we spatially shuffled the cells (i.e., randomized their location), applied
128 ARCOS to identify collective signaling events in the spatially permuted experiment, and recorded
129 the mean number of collective signaling events per cell (mean events per cell, MEC) across the
130 entire population. We repeated the sequence of random shuffling and ARCOS analysis 1,000 times
131 (Fig. 1E) and recorded: (A) the statistical significance - the fraction of times that the MEC of these
132 *in silico* spatially permuted experiments were equal or exceeded the MEC of the observed (un-
133 permuted) experiment, and (B) the magnitude - the mean ratio between the experimentally
134 observed MEC and each of the *in silico* spatially permuted MEC. All replicates, but one (11/12),
135 showed significant elevation in magnitude of MEC, by a factor of 1.2-3.3 fold in respect to the *in*
136 *silico* permuted experiments, indicating that the collective signaling events were a local property
137 of this multicellular system (Fig. 1F). Altogether, our data suggests that local cell-cell information
138 transfer integrates in space and time to form multicellular communities of Ca^{2+} signal propagating
139 blood progenitors in live intact *ex vivo* cultured LGs.

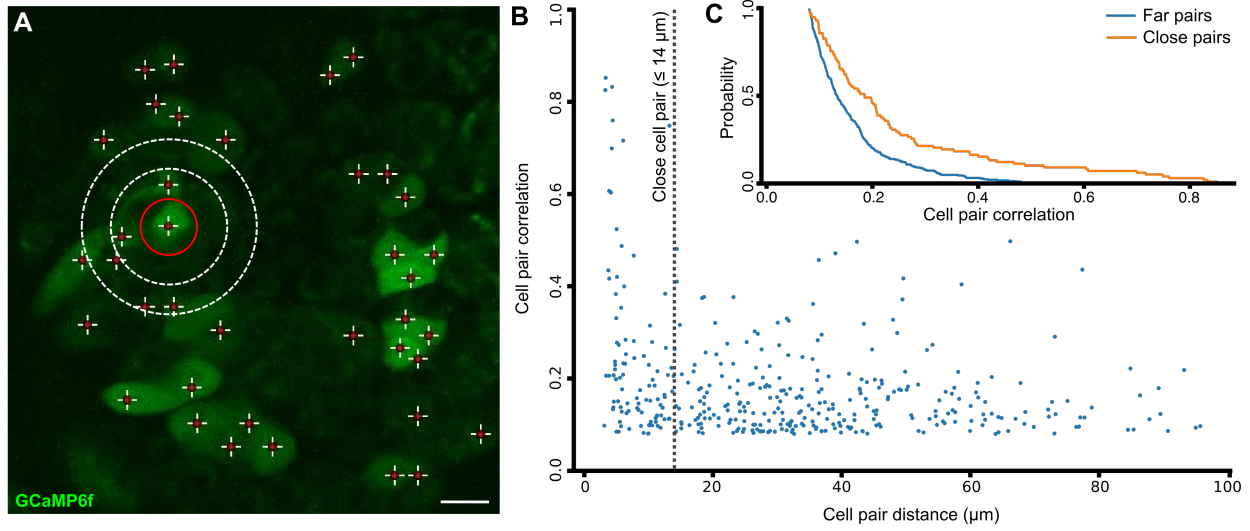
140

141 **Gap junctions mediate the propagation of Ca²⁺ signals in blood progenitor communities**

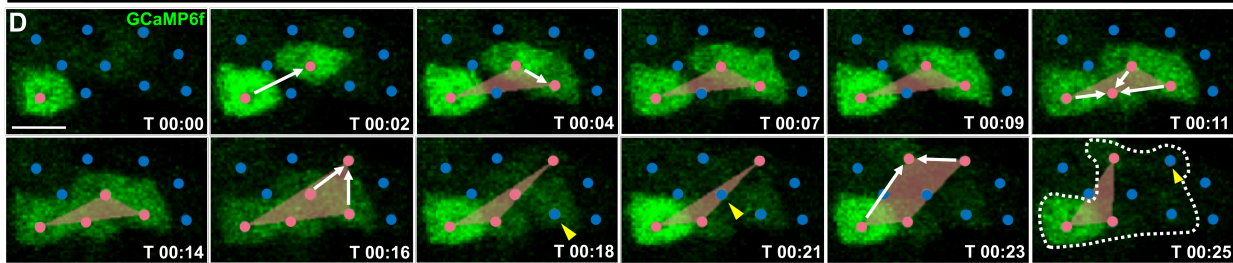
142 We previously demonstrated that gap junctions were required for cell-to-cell Ca²⁺ propagation
143 between the blood progenitors in the *Drosophila* LG (9). To assess the role of gap junctions in the
144 formation of intercellular communities, we analyzed *ex vivo* cultured LGs using live imaging under
145 different conditions where gap junctions were perturbed. Specifically, we used both a genetic and
146 a pharmaceutical-based approach to disrupt gap junction-mediated communication between blood
147 progenitors. First, we used an RNA interference (RNAi) approach to knock down the expression
148 of the gap junction protein Innexin 4, known by its gene name *zero population growth*, or *zpg* (14).
149 We have previously shown that *Zpg* is the main gap junction channel mediating Ca²⁺ signaling
150 between blood progenitors (9). Second, we used the gap-junction blocker known as carbenoxolone
151 (CBX). We performed RNAi-mediated knockdown of *zpg* (N = 8), a low dose CBX treatment
152 (3.125 μM; N = 3), a high dose CBX treatment (12.5 μM, N = 4), or a control where we first
153 treated with 100 μM CBX and then washed it out (N = 4). Analysis of these different treatment
154 groups showed that gap-junction inhibition led to a drastic decrease in the fraction of experiments
155 with significant local communities (Fig. 1G), the magnitude of collective signaling communities
156 (Fig. 1H), and the intercellular signaling propagation speed between adjacent cells (Fig. 1I).
157 Intriguingly, washout experiments that were previously shown to rescue the network properties
158 and cell-cell propagation (9), did not rescue the fraction of collective signaling-event communities
159 (Fig. 1G), but did rescue the magnitude of communities (Fig. 1H) and the intercellular signaling
160 propagation speed between adjacent cells in a transient community (termed *intercellular signaling*
161 *propagation speed*, Fig. 1I). This suggests that perturbation of gap junction-mediated
162 communication may have a long-lasting effect on the signaling community that persists even after
163 CBX is removed. The association between the LG's mean cell activation rate (i.e., frequency of
164 cell activation), mean local cell density, and the MEC rate, meaning the mean frequency that a cell
165 participates in a transient community, were maintained for most gap junction inhibition

166 perturbations (Fig. S4A-C). However, Zpg depletion (using RNAi) or inhibition (using CBX) led
167 to increased cell activation, i.e., higher frequency of Ca^{2+} spikes, but reduced MEC rate for the
168 same activation level (Fig. S4D), suggesting a compensation mechanism where Zpg-depleted or
169 inhibited cells try to compensate for reduced cell-cell communication capacity by increasing their
170 activity. These results validate the critical role of gap junctions in the formation of Ca^{2+} -based
171 intercellular communities.

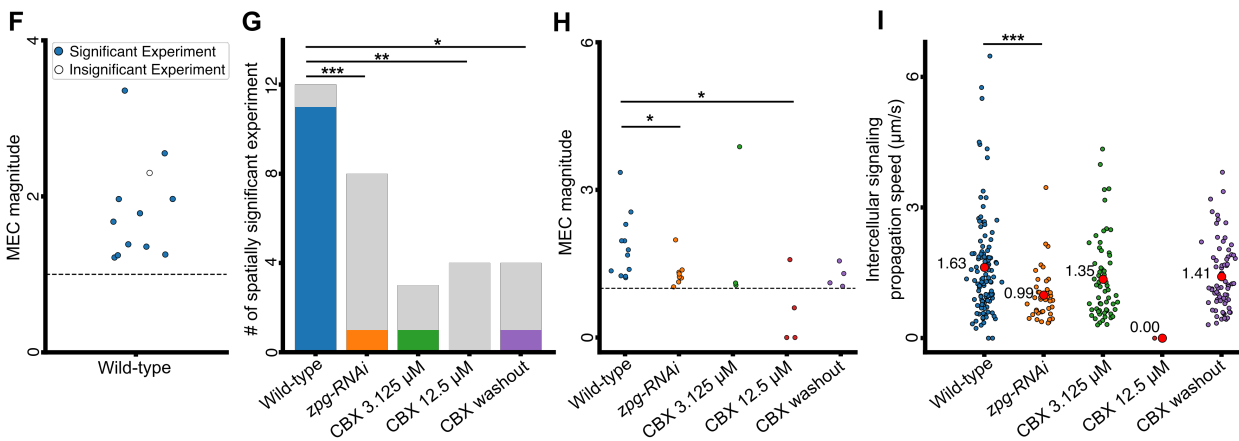
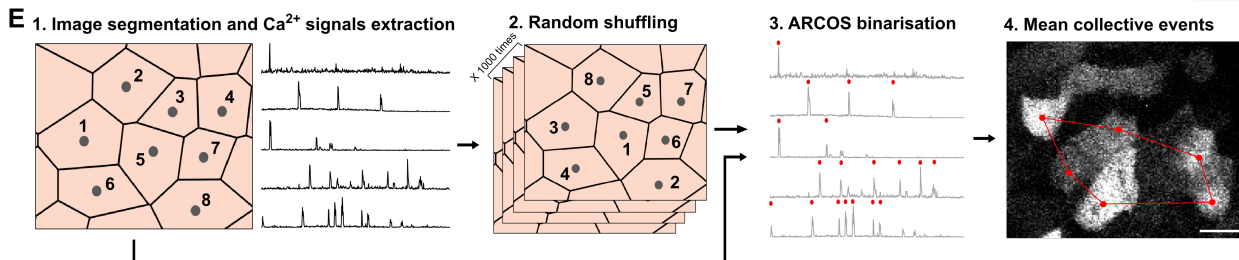
Analysis of Ca²⁺ cell pair synchronization in blood progenitors



Visualizing the evolution of a local transient signaling community



Statistical analysis



172

173 **Figure 1. Blood progenitor cell-cell communication forms communities of propagative Ca²⁺**
 174 **signaling. (A)** Representative confocal image showing Ca²⁺ signaling activities in blood progenitors of a

175 LG visualized using GCaMP6f (in green). Red crosses indicate the center of individual cells. White
176 circles indicate adjacent blood progenitors to the cell marked by the red circle, at distances of 7 μm and
177 14 μm from it correspondingly (see also Video S1). Scale bar = 10 μm . **(B)** Spatial analysis of blood
178 progenitor pairs that showed a statistically significant correlation ($p < 0.05$) in their temporal Ca^{2+} signals.
179 Each data point (blue) represents a cell pair. Cell pairs Ca^{2+} Pearson correlation was correlated with the
180 cell pairs distance. $N_{\text{cells}} = 57$, $N_{\text{pairs}} = 385$, Pearson correlation between cell pair Ca^{2+} correlation and
181 distance = -0.244, p -value = 0.003. See also Fig. S1A for an analysis of all cell pairs. **(C)** Cumulative
182 distribution of Pearson correlation of the close (orange; $N = 98$, $\mu = 0.246$, $\sigma = 0.187$) and far (blue; $N =$
183 287 , $\mu = 0.160$, $\sigma = 0.084$), significantly Ca^{2+} correlated blood progenitor pairs (same pairs as in B). Each
184 value $F_g(x)$ in the plot is the probability of a pair in group g to have a Pearson correlation coefficient
185 greater than x . Kruskal-Wallis statistical test verified a significant difference between the two
186 distributions (p -value < 0.0001). See also Fig. S1B for an analysis of all cell pairs. **(D)** Representative
187 confocal images showing a Ca^{2+} signaling propagation event, detected by ARCOS, which defined a
188 transient community involving 6 blood progenitors (see Results text and Methods). GCaMP6f is labeled
189 in green. The center of each cell is marked in red (active, i.e., showing Ca^{2+} influx) or blue (inactive).
190 Time (T , in second) is annotated in each frame. Orange polygons visualize the cell centers transiently
191 participating in a community in each frame. White arrows indicate the inclusion of new activated cells in
192 the community, yellow arrowheads indicate the deactivation and exclusion of cells from the community.
193 All the cells that participate in the community throughout its evolution are marked in the last frame ($T =$
194 $00:25$) in a dashed white polygon. Scale bar = 5 μm . **(E)** Schematic of the spatial shuffling analysis (see
195 also Methods). (1) Single-cell segmentation and extraction of Ca^{2+} time series. (2) Random spatial
196 shuffling of the Ca^{2+} time series of all cells, repeated 1000 times, correspondingly generating spatially
197 permuted experiments. (3) ARCOS binarization: Ca^{2+} peak detection (red). (4) ARCOS community
198 detection (red, white is GCaMP6f). Recording of the mean collective events per cell (MEC) and statistical
199 comparison of MEC for observed versus *in silico* permuted experiments. Scale bar = 5 μm . **(F)** Analysis
200 of MEC magnitude ($N = 12$ LGs). Mean ratio between MEC of the observed and the *in silico* permuted
201 experiments. The ratio of value 1 (dashed horizontal line) implies no change in the magnitude. The
202 bootstrapping significance test showed spatial significance for 11/12 LGs (color-filled circles). **(G-I)** Gap
203 junction inhibition experiments. Wild-type LGs ($N = 12$), RNAi-mediated *zpg* knockdown ($N = 8$), 3.125
204 μM CBX ($N = 3$), 12.5 μM CBX ($N = 4$), and CBX washout ($N = 4$). Statistical analyses: * - $p < 0.05$, **
205 - $p < 0.01$, *** - $p < 0.001$, **** - $p < 0.0001$. **(G)** Spatially significant experiments. For each
206 experimental condition, gray indicates the number of insignificant and color indicates the number of
207 significant LGs. Significance was determined using Fisher's exact test. **(H)** Analysis of MEC magnitude.
208 Each data point corresponds to one LG. Significance was determined using the Kruskal-Wallis test to
209 evaluate the differences between the wild-type and the other conditions. **(I)** Analysis of intercellular
210 signaling propagation speed between adjacent cells in a community. Each data point (red) represents the
211 average cell-cell signaling propagation speed calculated according to the relative activation timing
212 between adjacent pairs in each transient community (see Methods). Wild-type ($N = 113$ communities,
213 mean information spread $\mu = 1.63$ $\mu\text{m}/\text{second}$), RNAi-mediated *zpg* knockdown ($N = 39$, $\mu = 0.99$
214 $\mu\text{m}/\text{second}$), 3.125 μM CBX ($N = 62$, $\mu = 1.35$ $\mu\text{m}/\text{sec}$), 12.5 μM CBX ($N = 1$, $\mu = 0$ $\mu\text{m}/\text{second}$), and
215 CBX washout ($N = 71$, $\mu = 1.41$ $\mu\text{m}/\text{second}$). Statistical significance was determined using the Kruskal-
216 Wallis test to evaluate the differences between the wild-type and the other conditions.

217

218 **Recurrent activation of communication communities forms hotspots of local information** 219 **processing hubs**

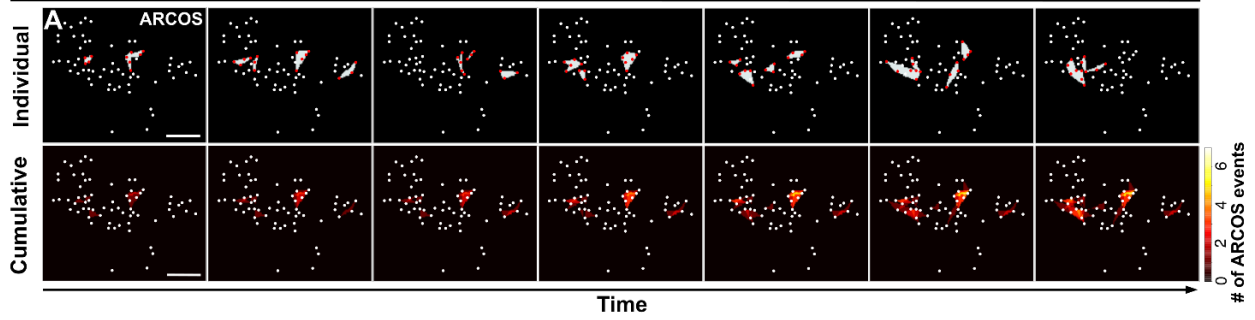
220 We next asked whether the same cells participate in multiple (transient) signaling communities, which,
221 if true, could suggest that these communities act as signaling communication “hubs” that repeatedly

222 receive and spread information to synchronize the multicellular network. To quantitatively assess this
223 possibility in wild-type LGs, we recorded for each cell the number of times it participated in signaling
224 communities. Visualization of the number of times each cell participated in a community revealed
225 spatial heterogeneity with recurrent activation of specific communities, that we call “hotspots”,
226 involving groups of spatially adjacent cells with enriched participation in signaling communities with
227 respect to the population (Fig. 2A, Fig. S5A-E, criteria for hotspot identification are detailed in the
228 Methods). We identified hotspots that met these criteria in 9 out of the 12 wild-type (non-treated)
229 LGs. The number of hotspots per LG ranged between 1 to 3 with each containing between 3 to 15
230 cells. To verify that hotspots were not a mere consequence of increased cell activation we devised a
231 bootstrapping-based statistical test (Fig. 2B-D). First, we matched and replaced at least 50% of the
232 cells in the hotspot with other cells in the same experiment that did not take part in the hotspot and
233 had, at minimum, the same amount of activations. Second, we switched the Ca^{2+} time series for each
234 pair of matched hotspot and non-hotspot cells, and then detected collective signaling events in this *in*
235 *silico*, spatially permuted, experiment (Fig. 2D). Third, we recorded the MECs for cells participating
236 in the hotspot of the *in silico* permuted experiment. We repeated these steps of switching “hotspot”
237 with non-hotspot cells with at least the same number of Ca^{2+} activation, up to 1,000 times for each
238 hotspot, recorded the difference between experimentally observed hotspots and their *in silico*
239 permuted versions, and determined the statistical significance. Statistical significance was determined
240 by calculating the fraction of permutations where the hotspot MEC values in the *in silico* experiments
241 were equal to or exceeded the MEC values of the observed (wild-type, non-permuted) experiment.
242 This analysis showed a dramatic decrease in the MEC following spatial permutation (Fig. S5),
243 statistically validating 8 of 14 hotspots, spread over 5 of the 12 live intact *ex vivo* cultured LGs (Fig.
244 2E). Qualitative observation of the validated hotspots locations did not identify a typical spatial
245 pattern in respect to the LGs. Gap-junction perturbations, even after washout, showed reduced
246 numbers of validated hotspots (Fig. 2E).

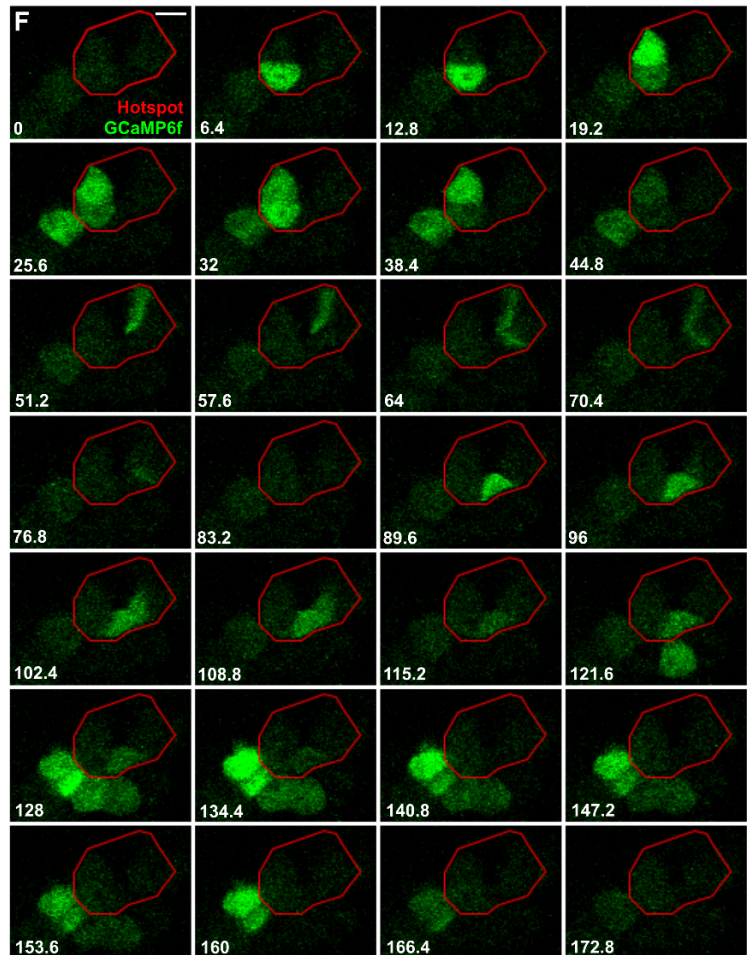
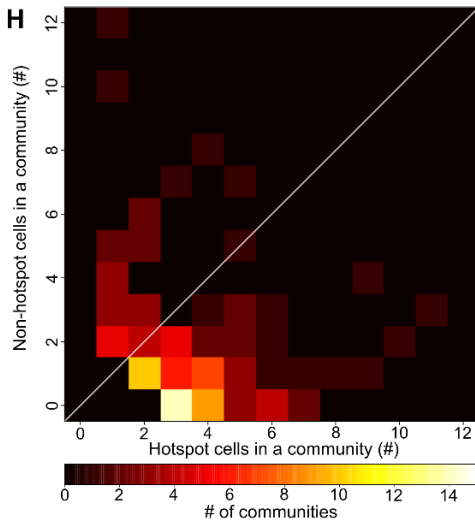
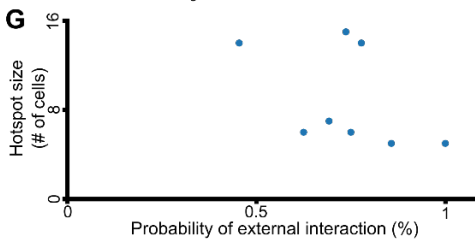
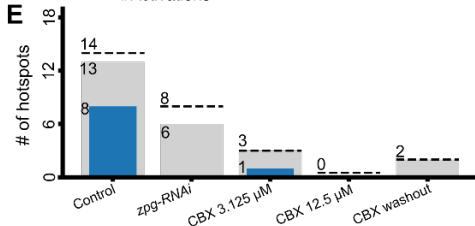
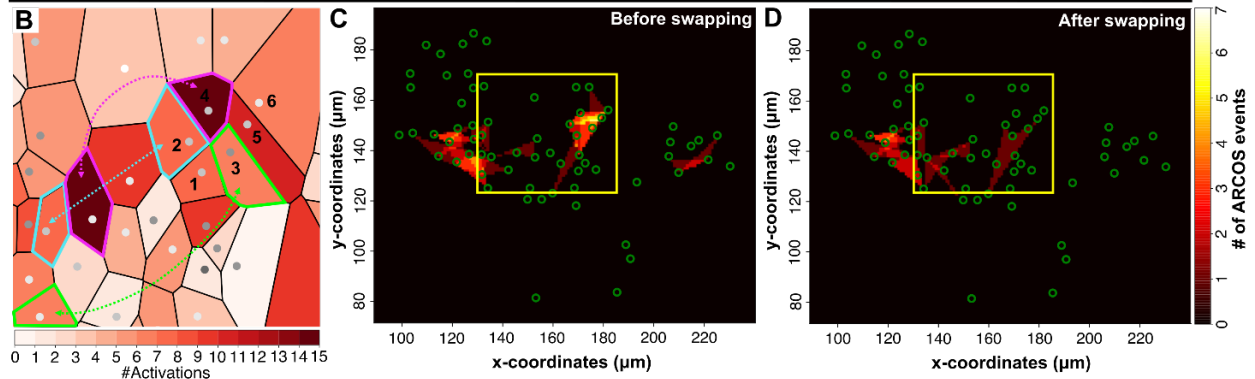
247 Our findings raised two important questions regarding the interaction of hotspots with their
248 environment. First, do hotspots function as self-contained groups of cells, interacting predominantly
249 within their enclosed local surroundings? Second, do hotspots initiate the spread of information, or
250 are they more responsive to incoming non-hotspots external signals? Following the evolution of a
251 transient community showed alternating interactions between cells inside and outside a hotspot (Fig.
252 2F). To systematically decipher the interactions between hotspots and their surrounding environment

253 we analyzed the spatiotemporal communication patterns of all the validated hotspots that were pooled
254 across the wild-type LGs (N = 8 hotspot). To quantify the interactions of hotspots with their
255 surrounding cells, we calculated each hotspot its probability of engaging with cells outside the hotspot
256 through common transient communities (Methods). The majority of hotspots (7 out of 8) interacted
257 with non-hotspot cells in more than half of their transient communities, this interaction was
258 independent of the size of a hotspot (Fig. 2G), and was dominated by communities that involved 2-4
259 cells within the hotspot and 1-2 cells external to the hotspot (Fig. 2H). Specifically, 70% of hotspot
260 communities had at least one non-hotspot cell involved, and 76% of these communities involved
261 more hotspot cells than non-hotspot cells (Fig. 2H). These interactions of a hotspot with its
262 surrounding cells did not have a systematic direction, starting from hotspot cells outwards or initiating
263 externally from adjacent non-hotspot cells (Fig. S6, Methods). Furthermore, we did not identify cells
264 that repeatedly initiated a hotspot's transient communities, suggesting stochasticity in hotspot
265 initiation. These observations established the existence of gap-junction-mediated communication
266 “hotspots”, where recurrent Ca^{2+} communities coalesce into larger communication hubs that
267 repeatedly spread and retrieve information throughout the blood progenitors.

Recurring communities reveal communication hotspots in the blood progenitor population



Bootstrapping-based *in silico* spatially permuted experiments statistically validates hotspots



269
270 **Figure 2. Recurrent activation of communities forms hotspots that act as local information hubs.**
271 (A) Representative time-lapse images showing the formation of hotspots over time. A hotspot is defined
272 by recurring transient communities (see Methods). Top panels: transient communities (marked by colored
273 polygons, red dots mark activated blood progenitors) in a wild-type LG. Bottom panels: the integrated
274 number of transient communities over time. Each white dot represents an individual blood progenitor.
275 Each panel corresponds to its matching top panel. Scale bar = 15 μm . (B) Single-cell Voronoi tessellation,
276 corresponding to the yellow region of interest shown in panels C and D, and illustrating the
277 bootstrapping-based *in silico* permutation experiment (see Methods). The color of each cell (polygon)
278 reflects the number of activations (i.e., calcium spikes) each cell exhibits. Six cells that participate in a
279 hotspot are numbered and dashed color-matched arrows indicate cell swapping. The swapping is
280 performed for cell pairs with similar activation, where one cell is within and the other outside the hotspot
281 (see Methods). (C-D) Representative field of view showing the integrated number of transient
282 communities each cell participated in over time (#ARCOS events) before (C) and after (D) *in silico*
283 permutation (see B). Green circles: the center location of each blood progenitor. Brighter areas indicate
284 more occurrences of communities. The yellow region of interest marks the hotspot that is also shown in
285 B. (E) Hotspot statistics. Hotspots were pooled across experiments according to the experimental
286 condition. Dashed line - pooled number of hotspots. Gray - pooled number of hotspots with sufficient
287 data for statistical analysis. Blue - number of statistically significant validated hotspots. Hotspot
288 significance was determined according to 100-1000 different *in silico* permutation experiments with a
289 bootstrapping significance threshold of 0.05. (F) Time-lapse evolution of a representative hotspot. The
290 hotspot was defined according to the integrated number of transient communities per cell across the
291 experiment (red polygon; see Methods). Transient communities involve cells within and outside the
292 hotspot. GCaMP6f labeled in green. Scale bar = 5 μm . (G) The probability of hotspot cells interacting
293 with cells outside the hotspot through common transient communities as a function of the hotspot's size
294 (i.e., the number of cells in the hotspot). The analysis included the 8 statistically verified hotspots pooled
295 across all wild-type LGs. (H) Histogram of the number of hotspot cells (x-axis) and non-hotspot cells (y-
296 axis) in communities that define the hotspots - each observation used for this histogram is defined by a
297 community. White diagonal ($y = x$) indicates an equal proportion between hotspot to non-hotspot cells.
298
299

300 **Gradual formation of communication communities and their recurrent activation during** 301 **LG development**

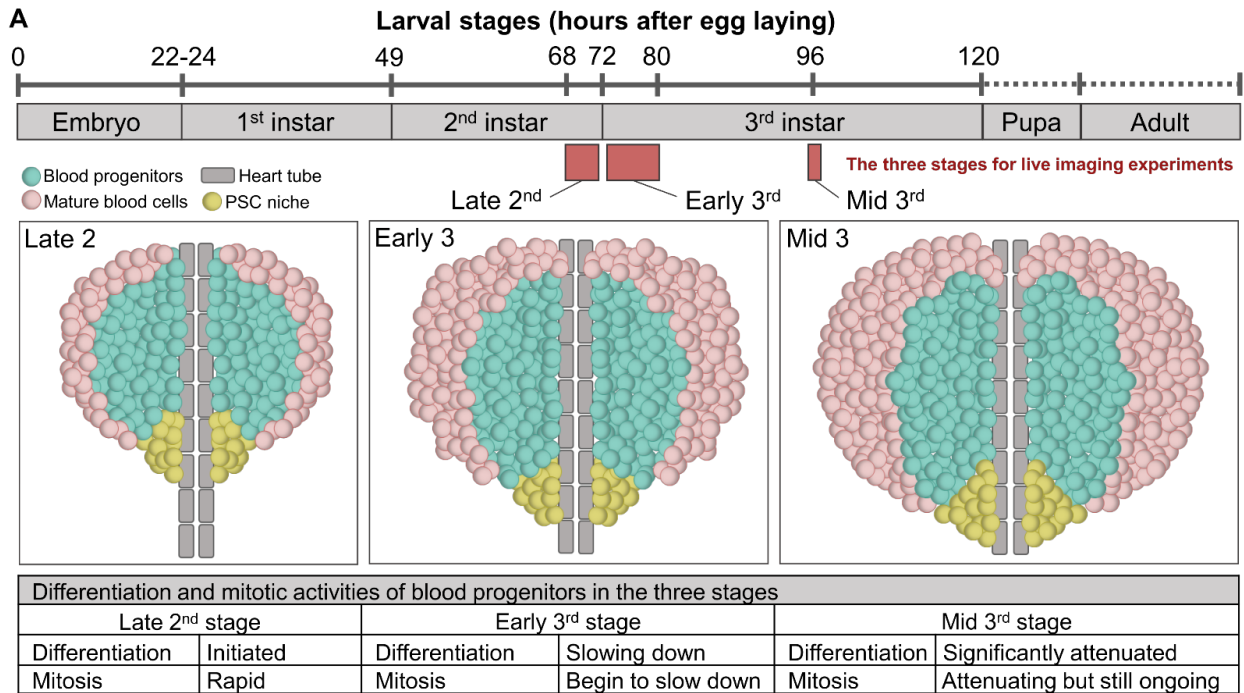
302 In flies, hematopoiesis is subject to developmental regulation, with blood progenitors exhibiting
303 distinct behaviors at different larval stages (15, 16). Specifically, cell proliferation and
304 differentiation show distinct patterns at different points along the developmental timeline (Fig.
305 3A) (16). For example, the differentiation of mature blood cells starts around the mid- to late-
306 second instar transition and peaks around the mid-second to mid-third instar larval stages (10, 15,
307 16). The level of mature blood cell differentiation gradually declines as the LG develops and
308 becomes significantly attenuated upon entry into the mid-third instar stage (Fig. 3A) (10, 16). In
309 contrast, cell proliferation in the blood progenitors peaks earlier, during the first- to second-instar
310 stages, when the progenitor repertoire rapidly expands (15, 16). Shortly after the onset of

311 differentiation, the rate of cell proliferation slows down but remains active until the mid-third
312 instar stage (Fig. 3A) (17).

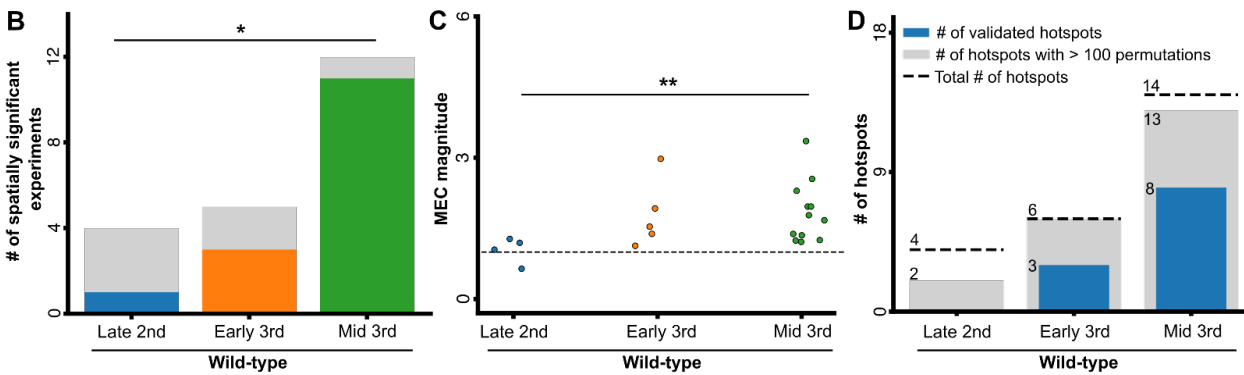
313 We previously showed that Ca^{2+} signaling appeared to evolve over larval development,
314 correlating with the differentiation activity of progenitors (9). Specifically, we observed lower
315 Ca^{2+} signaling propagation between neighboring cells and a reduced connectivity of the Ca^{2+}
316 signaling network during early larval stages (9). To understand how Ca^{2+} signaling communities
317 develop during hematopoiesis when progenitors show distinct proliferation and differentiation
318 patterns (Fig. 3A), we expanded our analysis to the earlier stages of the late-second and early-
319 third larval stages. Our analysis characterized a gradual build-up of signaling communities, in
320 terms of both quantity and complexity, over the course of blood progenitor development.
321 Specifically, both the fraction of experiments with significant local communities (Fig. 3B) and
322 the magnitude of MEC (Fig. 3C) increased across the three stages in wild-type LGs. In contrast,
323 RNAi-mediated *zpg* knockdown induced a decrease in both parameters of signaling communities
324 (Fig. 3E-F), suggesting that the emergence of signaling communities was perturbed. Hotspots
325 analysis showed a similar trend of gradual emergence of recurrent Ca^{2+} communities along the
326 developmental trajectory with 0/4 statistically validated hotspots in the late-second, 3/6 in the
327 early-third, and 8/14 in the mid-third stage (Fig. 3D). In contrast, no (0) hotspots were validated
328 across all developmental stages of the *Zpg*-depleted LGs (Fig. 3G). Taken together, our data
329 suggests that signaling communities and their recurrent activation (i.e., hotspots) emerge during,
330 and evolve over, the course of larval development and that gap junctions are required for the
331 developmental progression of these Ca^{2+} signaling communities in blood progenitors. This is
332 also consistent with our previous observation showing that *Zpg* depletion increases blood cell
333 differentiation (9), supporting a model where signaling communities coordinate blood progenitor
334 behavior to maintain LG homeostasis during development.

335

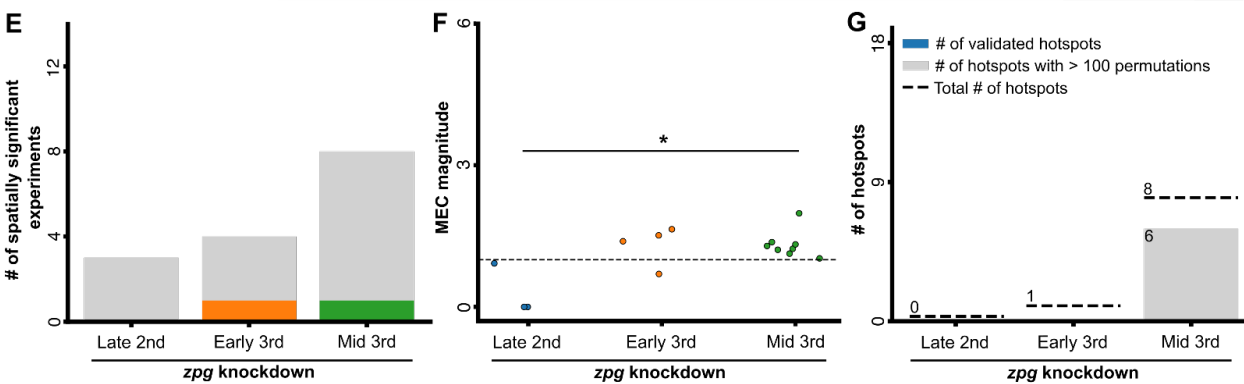
Lymph gland development across multiple larval stages in *Drosophila*



Developmental progression of hotspots



Zpg-mediated communication is required for the developmental progression of hotspots



336
337
338
339

Figure 3. Gradual formation of communication communities during development. (A) Lymph gland development throughout *Drosophila* larval stages (see Methods). (B-D) Analyses of wild-type LGs from

340 the late-second instar stage (N = 4), early-third instar stage (N = 5), and mid-third instar stage (N = 12).
341 **(B)** Number of spatially significant experiments. For each experimental condition, gray indicates the
342 number of insignificant and color indicates the number of significant LGs. Significance was determined
343 using Fisher's exact test. **(C)** MEC magnitude. Each data point corresponds to a single LG. Significance
344 was determined using the Kruskal-Wallis test to evaluate the differences between the different
345 developmental stages. **(D)** Hotspots statistics. Dashed line - pooled number of hotspots. Gray - pooled
346 number of hotspots with sufficient data for statistical analysis. Blue - number of statistically significant
347 validated hotspots. Hotspot significance was determined according to 100-1000 different *in silico*
348 permutation experiments with a bootstrapping significance threshold of 0.05. **(E-G)** Analyses of RNAi-
349 mediated *zpg* knockdown LGs from late-second instar stage (N = 3), early-third instar stage (N = 4), and
350 mid-third instar stage (N = 8). **(E)** Quantification of the number of spatially significant experiments in
351 blood progenitors. See B. **(F)** Analysis of MEC magnitude. See C. **(G)** Number of validated hotspots per
352 developmental stage. See D.
353

354 Discussion

355 There are numerous examples in the literature reporting synchronization and collective events in
356 the context of cell signaling and behavior (13, 18, 19). A critical question that has remained
357 underexplored is how does global, tissue-scale synchronization emerge from local cell-cell
358 communication? More specifically, what are the intermediary steps involved in reaching the final
359 synchronization state? In an attempt to provide some insight into the answers to these questions,
360 we have previously described how endothelial monolayers synchronize Ca^{2+} signaling by
361 gradually transitioning from local to global information spread (19). Other studies reported
362 signaling waves propagating across long distances in a variety of systems and in the context of
363 diverse functions (13, 20-22). However, these studies did not pinpoint a specific intermediate
364 spatial scale between single-cell and collective signaling. Here, using *Drosophila* hematopoiesis
365 as our model system, we were able to identify such an intermediate spatial scale. Our work
366 elaborates on our previous findings that described the important role played by gap junctions in
367 coordinating cellular signals in the LG (9). We now show that an intermediate spatial scale
368 exists, involving transient gap junction-mediated Ca^{2+} signaling in the form of multicellular
369 communities. Similar scale collective events were previously reported in the context of Erk
370 signaling in epithelial cells, and Ca^{2+} signaling in the Madin-Darby canine kidney epithelium
371 (13) suggesting that this could be a universal way to collectively organize the signaling activity
372 of individual cells in a multicellular system.

373 A key feature in some of these transient communities was recurrent activation events that formed
374 larger communication processing hubs that we call signaling hotspots. These hotspots had
375 several important functional characteristics: 1) Their formation required the activity of Zpg-
376 based gap junctions. 2) They acted as information hubs that were able to induce (i.e., transmit)
377 and process (i.e., receive) collective signaling using mechanisms that operated both within
378 (intrinsically) and outside (extrinsically) of the hotspot. 3) They exhibited repetitive interactions
379 with their environment and were spatially heterogeneous. 4) There was an increased incidence of
380 hotspots as the LG evolved and developed consistent with a role in the emergence of collective
381 cell behavior. Each of these characteristics of the hotspots played an important functional role in
382 shaping the signaling landscape within the LG. Overall, these findings reveal a novel mechanism
383 whereby local cell-cell signaling propagation, through gap junctions, progresses into

384 intermediate multicellular communities that integrate local information to achieve global
385 population-wide synchronization during fly hematopoiesis.

386 Our observation that hotspots self-organize as information processing hubs in the blood
387 progenitor population suggests that the hotspots perform a function that bears general
388 resemblance to that performed by pacemaker cells, at the multicellular scale. A characteristic of
389 pacemaker cells is their ability to coordinate the electrical or Ca^{2+} signaling activity of individual
390 cells to guide collective decisions (18, 23, 24). Multicellular structures that are functionally and
391 morphologically similar to pacemaker cells appear across diverse tissues, including Cajal
392 interstitial cells in the gut (25), a sinoatrial node in the heart (24), and preBötC cells in the brain
393 stem (26), indicating that it is a conserved module in living systems to regulate systemic
394 homeostasis. We note three features of blood progenitor hotspots that resemble those found in
395 pacemaking cells. First, as we previously proposed, blood progenitors form a small-world Ca^{2+}
396 signaling network (9), where most cells are separated from each other by a small number of cell-
397 to-cell transmission events thanks to a small subgroup of cells with high connectivity compared
398 to other cells (12). Here, using ARCOS and *in silico* spatial permutation analysis, we directly
399 demonstrated the existence of such hub-like network structures, or hotspots, within the blood
400 progenitor population. Second, a well-known feature of pacemaker cells is their ability to
401 integrate and segregate information between cells that are either external or internal to their
402 signaling hub (27-29). Our study quantitatively illustrates that Ca^{2+} signaling in blood
403 progenitors is organized into hotspots that are able to both receive and send information. Third,
404 there are several functional analogies between the hotspots found in blood progenitors and
405 cardiac pacemaker cells found in sinoatrial nodes. These include: (A) transfer of information
406 across large distances and the ability to fine-tune the activities of a large group of cells (24), (B)
407 highly synchronized multicellular activity that is often tied to function (9, 24, 30), (C)
408 coordinated cell behavior that is dependent on gap junctions (9, 30), (D) self-organization and
409 synchronization of local heterogeneous Ca^{2+} signals (24), and (E) intracellular Ca^{2+} signals in
410 both systems are controlled by the same molecular machinery including gap junctions (9, 23,
411 30), SERCA pumps (9, 31), and ryanodine receptors (10, 31). These observations highlight
412 similar design principles, both conceptual and functional, that allow LG blood progenitor
413 hotspots and cardiac pacemaker cells to coordinate cells within a population.

414 Signaling hotspots highlight the spatial heterogeneity in intercellular Ca^{2+} information processing
415 in the developing LG. How such heterogeneity develops in seemingly homogenous blood
416 progenitors remains unknown. Heterogeneity in intercellular communication, even in the same
417 cell population, can originate from intrinsic cell-to-cell variation in gene expression levels or
418 protein modifications (32-34). Indeed, single-cell transcriptomic analysis on LGs showed that
419 blood progenitors, which were previously considered as a homogenous population, exhibited a
420 large variability in their gene expression profiles (35). The differences in their gene enrichment
421 were used to classify progenitors into 6 main sub-clusters that showed distinct spatial distribution
422 and gene expression profiles (35), suggesting that the difference in gene expression could
423 contribute to the heterogeneity of Ca^{2+} signaling. Beyond gene expression or protein
424 modifications, the positioning of the cells within the LG and in relation to other organs may lead
425 to spatial heterogeneity between hotspots, by supporting different modes of cell-cell interaction
426 (36). However, we were not able to identify a stereotypic spatial pattern in the hotspot location.

427 The emergence of hotspots from oscillating blood progenitors required a mechanism that
428 coordinates their individual activities. Although we demonstrated that the function of Zpg-based
429 gap junctions was indispensable in this process, the underlying mechanism remains unclear. We
430 can envision several possible routes for the emergence of collective Ca^{2+} signaling hotspots in
431 the blood progenitor population. According to theoretical, physics, and neural-based studies,
432 routes giving rise to collective behaviors can be classified into four main categories (37): (A)
433 Pacemaker cells, in this context cells that fire rhythmic signals, entraining other cells to oscillate
434 or behave in a synchronized fashion (38). (B) Phase and/or frequency locking, where cells that
435 naturally oscillate at different frequencies synchronize their behaviors by adjusting their phases
436 and/or frequencies when coupled with other cells, a representative example being circadian
437 neurons (39-42). (C) Oscillator death, where mathematical approaches and synthetic genetic
438 clocks show that cells stop oscillating when coupled with other cells (37, 43). Therefore,
439 decreasing the coupling strength permits the emergence of synchronized behavior. (D) Dynamic
440 quorum sensing, where non-oscillatory cells start oscillating when a signaling molecule they
441 secrete exceeds a critical concentration threshold in their environment, an example being yeast
442 glycolytic oscillations (37). Comparing our data with the above four categories, we proposed that
443 hotspot emergence likely involves a hybrid mechanism with both pacemaker-like and
444 phase/frequency locking properties. First, we noticed that some progenitors were still able to

445 produce Ca^{2+} spikes even in the presence of a high concentration of CBX (9), indicating that
446 these cells spontaneously produce spikes without the need of neighbor connections. As discussed
447 in the previous section (Hotspots act as information hubs), the progenitor hotspots show
448 characteristics consistent with having pacemaker-like properties. Second, for the
449 phase/frequency locking property, we found that the complexity and incidence rate of hotspots
450 increased concomitant with animal development. This showed that hotspots are able to
451 accommodate or incorporate new cells in a developing progenitor population. Our previous
452 observations show that the number of gap junctions increased and the spiking frequency of blood
453 progenitors was modulated during LG development (9). These two lines of evidence suggest that
454 the newly incorporated cells, once coupled with other cells, changed their spiking frequency over
455 time, consistent with the phase/frequency locking phenomenon. Overall, we suggested that the
456 progenitor hotspots emerge by simultaneously utilizing the pacemaker-like and phase/frequency
457 docking mechanisms. Taken together, our findings align with other recent studies that reported
458 collective signaling in the spatial scale of multiple cells (13, 44, 45), suggesting a universal
459 mechanism to collectively organize the signaling activity of individual cells in a multicellular
460 system.

461

462 Materials and Methods

463 ***Drosophila* genetics, stocks, and maintenance**

464 All *Drosophila* stocks and crosses were maintained regularly on a standard cornmeal medium
465 (recipe from the Bloomington *Drosophila* Stock Center) in vials or bottles at 25°C. The blood
466 progenitor-specific Gal4 driver used was *Tep4-Gal4* (a kind gift from Dr. Lucas Waltzer,
467 Université Clermont Auvergne, France). Other lines used were: *UAS-GCaMP6f*
468 (RRID:BDSC_42747) and *UAS-zpg-RNAi* (RRID:BDSC_35607). Larvae were staged as
469 follows: eggs were first collected 6~8 hours after egg laying (AEL), late-second instar larvae
470 were collected 68-72 hours AEL, early-third instar larvae were collected 72-80 hours AEL, and
471 mid-third instar larvae (or wandering third instar larvae) were collected 96 hours AEL (9).

472

473 **Sample preparation and confocal imaging**

474 To prepare live LG samples, larvae in desired stages were washed using Phosphate-Buffered
475 Saline (PBS) three times (2 minutes each), quickly rinsed with 70% ethanol, washed again with
476 PBS three times (2 minutes each), and dissected in the *Drosophila* Schneider's medium (pre-
477 warmed to room temperature 10 minutes prior dissection; ThermoFisher Scientific, 21720001).
478 The dissected LG was mounted in the glass bottom dishes (MatTek Corporation, 35 mm, P35G-
479 0-14-C, non-coated), covered with a 1% agar pad (Agar A, Bio Basic, FB0010, prepared in the
480 Schneider's medium), and stabilized with 1% agar spacers to prevent LG compression during
481 live recordings (15). The dish was supplied with 2 ml Schneider's medium over the agar pad for
482 moisture and placed in a microscope incubator (TOKAI HIT, Catalog number: INU-ONICS F1)
483 that maintains the temperature at 25°C during imaging. LG optical sections spaced by 1.5µm
484 were imaged using a 40X oil immersion objective (numerical aperture 1.30, UPLFLN) on an
485 Olympus inverted confocal microscope (FV1000) with a temporal resolution ranging from 2.3-
486 6.7 seconds per frame (9).

487 To monitor real-time Ca²⁺ signals in blood progenitors, a genetically encoded Ca²⁺ sensor
488 GCaMP6f (peak excitation ~480 nm, peak emission ~510 nm) was expressed. Fiji (46) was used
489 to manually annotate circular ROIs around each progenitor cell according to the GCaMP6f

490 activity. Raw GCaMP6f intensity values were extracted at the ROIs at individual time points (z-
491 profile Fiji plugin) and exported to Excel (in .csv format). The obtained GCaMP6f signals of
492 each cell were normalized, $F'_t = (F_t - F_{\min}) / (F_{\max} - F_{\min})$ where F_t = raw GCaMP6f value at each
493 time point, F_{\min} and F_{\max} = minimum and maximum GCaMP6f values of a cell, respectively) (9,
494 15). Time-lapse recordings were processed in Fiji and Fluoview (Olympus FV10-ASW 4.2) and
495 the data was analyzed using Python. No stabilization or registration on images was performed.
496 Intensities represented mean gray values.

497 To block gap junctions, live dissected LGs were incubated in 50 or 100 μ M CBX (Sigma,
498 CG4790) for 15 minutes, mounted in the Schneider's medium with corresponding CBX
499 concentration, and imaged immediately (9). For the CBX-washout experiment, LGs were
500 incubated in 100 μ M CBX for 15 minutes, rinsed in the Schneider's medium twice (5 minutes
501 each), mounted, and imaged immediately (9). A 1mM CBX stock was stored at -20 °C. Imaging
502 settings were set identically across experiments.

503

504 **Transient communities detection and analysis**

505 We applied ARCOS (13) to detect and quantify the Ca^{2+} collective signaling events in blood
506 progenitors. We applied the ARCOS Python implementation (arcos4py, version 0.1.5) on the
507 normalized time series for each inspected LG. We set neighborhoodSize to 14 μ m, which represents
508 about two cell diameters. minClasz, the minimum initial size for a cluster to be identified as a
509 collective event, was set to 1. minTotalEventSize, the final size of the cluster at the end of the event,
510 was set to 3 cells. This way we enforced a minimum cluster size of 3 cells while allowing
511 asynchronous cell activations. nPrev, the maximal number of frames between different cell
512 activations, was configured empirically to a maximum time lag of 15 seconds according to the
513 temporal resolution. minDuration, the minimal time for a collective event, was set to 1 frame,
514 enabling the detection of short-term co-occurring activations. Binarization parameters were set
515 according to the default recommended values (13), with biasMet, smoothK and biasK set to
516 “runmed”, 3 and 51, respectively. To minimize the detection of false activations, peakThr and
517 binThr were empirically set to 0.3 and 0.4, respectively.

518 **Statistically validating local properties of collective signaling events**

519 We designed a bootstrapping-based statistical test to reject the null hypothesis that the collective
520 signaling events are non-local properties. This was achieved by repeating the following steps
521 1,000 times: (A) spatially shuffling the cells' time series, which is equivalent to randomizing the
522 cells' locations; (B) applying ARCOS to the spatially shuffled time series; (C) recording the
523 mean number of collective signaling events per cell (mean events per cell, MEC) across the
524 spatially shuffled cells. The statistical significance was calculated as the fraction of spatially
525 shuffled experiments where the MEC was equal to or exceeded the MEC of the observed (not
526 shuffled) experiment. The MEC magnitude was calculated as the mean ratio between the
527 experimentally observed MEC and the MEC of each of the spatially shuffled experiments, and
528 indicates the MEC fold change in respect to excluding the spatial organization.

529

530 **Mean local cell density and mean cell activation**

531 The *mean local cell density* was defined as the average number of cells within a square area of
532 $14 \times 14 \mu\text{m}^2$ surrounding each cell. The *mean activation rate* was defined as the average number
533 of activations per cell per minute. Both measurements were calculated according to the mean
534 value of all cells in each LG.

535

536 **Communities' intercellular signaling propagation speed**

537 The *intercellular signaling propagation speed* of a community was defined as the mean time
538 difference between the activation of adjacent cells as a function of the distance between these
539 cells ($\mu\text{m}/\text{second}$) in the context of the transient community. This community-specific
540 measurement was pooled across all LGs within each experimental condition. To avoid
541 confounding effects due to different temporal resolutions between experiments, we excluded
542 experiments that had temporal resolution outside the range of 2.32-4 seconds per frame. This
543 range maintains a sufficient and similar amount of LGs per treatment ($N_{wild\ type\ late\ 2nd} = 4$;
544 $N_{wild\ type\ early\ 3rd} = 5$; $N_{wild\ type\ mid\ 3rd} = 4$; $N_{zpg\ RNAi\ late\ 2nd} = 3$; $N_{zpg\ RNAi\ early\ 3rd} = 3$;
545 $N_{zpg\ RNAi\ mid\ 3rd} = 3$; $N_{CBX\ 3.125} = 2$; $N_{CBX\ 12.5} = 1$, $N_{CBX\ washout} = 4$).

546

547 **Hotspots analysis**

548 We defined LG_{\max} as the maximal number of transient communities in which a single cell
549 participated within a specific LG. We defined $LG_{\text{threshold}}$ as the maximum between 5 and LG_{\max} ,
550 and marked all cells that participated in at least $LG_{\text{threshold}}$ transient communities. For each
551 connected component (in the neighborhood graph) group of adjacent cells above this threshold
552 we calculated its convex hull and considered it as a *hotspot candidate*. To validate that a hotspot
553 was not a result of random effects nor physical confounding factors (see Methods: Confounders
554 analysis), we conducted a bootstrapping-based statistical test as follows. First, we matched at
555 least 50% of the hotspot cells with other non-hotspot cells from the same LG, where each of the
556 non-hotspot cells participated in at least the same number of transient communities as its
557 matching hotspot cell. Second, we swapped the Ca^{2+} time series of each matched pair of hotspot
558 and non-hotspot cells. Third, we employed ARCOS on the *in silico* spatially permuted LG to
559 detect collective signaling events. Fourth, we recorded the MEC for the permuted hotspot cells.
560 Fifth, we repeated these four steps for each hotspot up to 1000 times, hotspot candidates with at
561 least 100 different *in silico* spatially permuted LGs were considered for the bootstrapping-based
562 significance test. For each hotspot candidate, the statistical significance was determined as the
563 percentage of *in silico* permutations that yielded equal or greater MEC values compared to the
564 original non-permuted LG. A hotspot candidate with a p-value ≤ 0.05 was considered as a
565 *validated hotspot*.

566

567 **Interactions between hotspots and their surrounding environment**

568 We quantified the interaction between cells within hotspots and their adjacent non-hotspot cells,
569 and measured the temporal ordering of the cells' activation. *Hotspot community* was each
570 transient community that included at least one hotspot cell. For each hotspot, we calculated the
571 ratio between the number of hotspot communities involving both hotspot and non-hotspot cells
572 to the total number of hotspot communities (also including hotspot-exclusive cells). This ratio
573 represents the probability of hotspot cells interacting, via a transient community, with non-
574 hotspot cells.

575 The direction of interaction between hotspot and non-hotspot cells was defined as whether a
576 hotspot community was initiated by a hotspot or a non-hotspot cell. This analysis focused on
577 hotspot communities involving at least one non-hotspot cell. We defined two measurements for
578 directionality: (A) The fraction of hotspot communities that were initiated by hotspot cells. For

579 this measurement, we excluded hotspot communities that were initiated by both hotspot and non-
580 hotspot cells that appeared in the same time frame, because of the ambiguity to which cell
581 initiated the community. (B) For each hotspot transient community, we considered all cell pairs
582 comprising one hotspot cell and one non-hotspot cell, within a distance $\leq 14 \mu\text{m}$ from one
583 another. We calculated the *transmission probability* as the fraction of such pairs where the
584 hotspot cell was activated before the non-hotspot cell.

585 The hotspot size was defined as the number of cells participating in the hotspot. The proportion
586 of hotspot cells in transient communities was defined as the fraction of hotspot cells in a
587 community. This proportion was averaged across all hotspot communities to define the average
588 proportion of hotspot cells in transient communities, which was used as the expected probability
589 of a hotspot cell to be the initiator of a hotspot transient community, under the assumption of
590 random activation order of cells within a community.

591

592 **Statistical analysis**

593 Pearson correlation (`scipy.stats.pearsonr`) was used to measure the correlation between the Ca^{2+}
594 signals of blood progenitors (see Fig. 1B-C) and the correlation between MEC rate, mean local
595 cell density, and mean cell activation rate (see Fig. S3, Fig. S4). Bootstrapping was applied in the
596 spatial shuffle analysis (e.g., Fig. 1E) and the hotspot shuffle analysis (e.g., Fig. 2C). Fisher's
597 exact test (`scipy.stats.fisher_exact`) was used to measure the differences between different
598 experimental conditions (treatments) in terms of the amount of spatially significant LGs (e.g.,
599 Fig. 1F-G, Fig. 3B, Fig. 3E). Fisher's exact test was chosen due to the small sample size in each
600 experimental condition, and due to the categorical nature of the data. Kruskal-Wallis test
601 (`scipy.stats.kruskal`) was used to measure the difference between the distributions of cell pair
602 Pearson correlation of Ca^{2+} signals (Fig. 1C, Fig. S1B), magnitude of MEC (Fig. 1H, Fig. 3C,
603 Fig. 3F), community-level information spread rate (Fig. 1I), and distance distribution comparison
604 (Fig. S4D) across experimental conditions. Non-parametric Kruskal-Wallis test was chosen due
605 to the varying sample sizes across different experimental conditions and due to the unknown
606 underlying distribution of our data. All significance tests were carried out with an α -value of
607 0.05, considering * - $p < 0.05$, ** - $p < 0.01$, *** - $p < 0.001$, **** - $p < 0.0001$.

608

609 **Software and data availability**

610 We are currently organizing our source code and will make it publicly available as soon as
611 possible (before journal publication).

612

613 **Funding and Acknowledgments**

614 The authors acknowledge the Bloomington *Drosophila* Stock Center. The authors thank Dr.
615 Lucas Waltzer for providing fly stocks. Research at the Zaritsky laboratory is supported by the
616 Israel Council for Higher Education (CHE) via the Data Science Research Center, Ben-
617 Gurion University of the Negev, Israel, by the Israel Science Foundation (ISF, grantNo. 2516/21),
618 by the Israel Ministry of Science and Technology (MOST), by the Wellcome Leap Delta Tissue
619 program, by the German-Israeli Foundation (GIF)-Nexus, and by the Rosetrees Trust. Research
620 in the lab of G.T. is supported by the Canadian Institutes of Health Research (Project Grant PJT-
621 156277). K.Y.L.H is supported by a 4-Year Doctoral Fellowship from the University of British
622 Columbia. The authors thank Dr. Bo Sun, Dr. Dagan Segal, and Dr. Julia Mack for critically
623 reading the manuscript.

624 **Author Contribution**

625 AZ, SBD, and GT conceived the study. KYLH designed the experimental assay and performed
626 all experiments. SBD developed analytic tools, analyzed, and interpreted the data with the help
627 of KYLH. AZ and GT mentored SBD and KYLH. All authors wrote and edited the manuscript
628 and approved its content.

629 **Competing Financial Interests**

630 The authors declare no financial interests.

631

632 References

- 633 1. F. Julicher, S. Eaton, Emergence of tissue shape changes from collective cell behaviours.
634 *Seminars in cell & developmental biology* **67**, 103-112 (2017).
- 635 2. R. Mayor, S. Etienne-Manneville, The front and rear of collective cell migration. *Nature*
636 *reviews. Molecular cell biology* **17**, 97-109 (2016).
- 637 3. B. L. Bassler, How bacteria talk to each other: regulation of gene expression by quorum
638 sensing. *Current opinion in microbiology* **2**, 582-587 (1999).
- 639 4. M. G. Surette, M. B. Miller, B. L. Bassler, Quorum sensing in *Escherichia coli*,
640 *Salmonella typhimurium*, and *Vibrio harveyi*: a new family of genes responsible for
641 autoinducer production. *Proceedings of the National Academy of Sciences of the United*
642 *States of America* **96**, 1639-1644 (1999).
- 643 5. L. Capuana, A. Bostrom, S. Etienne-Manneville, Multicellular scale front-to-rear polarity
644 in collective migration. *Current opinion in cell biology* **62**, 114-122 (2020).
- 645 6. S. Toda, N. W. Frankel, W. A. Lim, Engineering cell-cell communication networks:
646 programming multicellular behaviors. *Current opinion in chemical biology* **52**, 31-38
647 (2019).
- 648 7. U. Banerjee, J. R. Girard, L. M. Goins, C. M. Spratford, *Drosophila* as a Genetic Model
649 for Hematopoiesis. *Genetics* **211**, 367-417 (2019).
- 650 8. C. J. Evans, T. Liu, J. R. Girard, U. Banerjee, Injury-induced inflammatory signaling and
651 hematopoiesis in *Drosophila*. *Proceedings of the National Academy of Sciences of the*
652 *United States of America* **119**, e2119109119 (2022).
- 653 9. K. Y. L. Ho, R. J. Khadilkar, R. L. Carr, G. Tanentzapf, A gap-junction-mediated,
654 calcium-signaling network controls blood progenitor fate decisions in hematopoiesis.
655 *Current biology : CB* **31**, 4697-4712 e4696 (2021).
- 656 10. J. Shim *et al.*, Olfactory control of blood progenitor maintenance. *Cell* **155**, 1141-1153
657 (2013).
- 658 11. J. Mathews, M. Levin, Gap junctional signaling in pattern regulation: Physiological
659 network connectivity instructs growth and form. *Developmental neurobiology* **77**, 643-
660 673 (2017).
- 661 12. E. Smedler, S. Malmersjo, P. Uhlen, Network analysis of time-lapse microscopy
662 recordings. *Frontiers in neural circuits* **8**, 111 (2014).
- 663 13. P. A. Gagliardi *et al.*, Automatic detection of spatio-temporal signaling patterns in cell
664 collectives. *The Journal of cell biology* **222** (2023).
- 665 14. R. Bauer *et al.*, Intercellular communication: the *Drosophila* innexin multiprotein family
666 of gap junction proteins. *Chemistry & biology* **12**, 515-526 (2005).
- 667 15. K. Y. L. Ho, R. L. Carr, A. D. Dvoskin, G. Tanentzapf, Kinetics of blood cell
668 differentiation during hematopoiesis revealed by quantitative long-term live imaging.
669 *eLife* **12** (2023).
- 670 16. J. Krzemien, J. Oyallon, M. Crozatier, A. Vincent, Hematopoietic progenitors and
671 hemocyte lineages in the *Drosophila* lymph gland. *Developmental biology* **346**, 310-319
672 (2010).
- 673 17. B. C. Mondal *et al.*, Interaction between differentiating cell- and niche-derived signals in
674 hematopoietic progenitor maintenance. *Cell* **147**, 1589-1600 (2011).

- 675 18. B. Sun, J. Lembong, V. Normand, M. Rogers, H. A. Stone, Spatial-temporal dynamics of
676 collective chemosensing. *Proceedings of the National Academy of Sciences of the United*
677 *States of America* **109**, 7753-7758 (2012).
- 678 19. A. Zamir *et al.*, Emergence of synchronized multicellular mechanosensing from
679 spatiotemporal integration of heterogeneous single-cell information transfer. *Cell systems*
680 **13**, 711-723 e717 (2022).
- 681 20. K. Aoki *et al.*, Propagating Wave of ERK Activation Orients Collective Cell Migration.
682 *Developmental cell* **43**, 305-317 e305 (2017).
- 683 21. N. Hino *et al.*, ERK-Mediated Mechanochemical Waves Direct Collective Cell
684 Polarization. *Developmental cell* **53**, 646-660 e648 (2020).
- 685 22. P. A. Gagliardi *et al.*, Collective ERK/Akt activity waves orchestrate epithelial
686 homeostasis by driving apoptosis-induced survival. *Developmental cell* **56**, 1712-1726
687 e1716 (2021).
- 688 23. K. T. Moortgat, T. H. Bullock, T. J. Sejnowski, Gap junction effects on precision and
689 frequency of a model pacemaker network. *Journal of neurophysiology* **83**, 984-997
690 (2000).
- 691 24. R. Bychkov *et al.*, Synchronized Cardiac Impulses Emerge From Heterogeneous Local
692 Calcium Signals Within and Among Cells of Pacemaker Tissue. *JACC. Clinical*
693 *electrophysiology* **6**, 907-931 (2020).
- 694 25. M. Y. Lee *et al.*, Transcriptome of interstitial cells of Cajal reveals unique and selective
695 gene signatures. *PloS one* **12**, e0176031 (2017).
- 696 26. J. L. Feldman, K. Kam, Facing the challenge of mammalian neural microcircuits: taking a
697 few breaths may help. *The Journal of physiology* **593**, 3-23 (2015).
- 698 27. N. Takahashi, T. Sasaki, W. Matsumoto, N. Matsuki, Y. Ikegaya, Circuit topology for
699 synchronizing neurons in spontaneously active networks. *Proceedings of the National*
700 *Academy of Sciences of the United States of America* **107**, 10244-10249 (2010).
- 701 28. M. Rubinov, O. Sporns, Complex network measures of brain connectivity: uses and
702 interpretations. *NeuroImage* **52**, 1059-1069 (2010).
- 703 29. A. L. Barabasi, Z. N. Oltvai, Network biology: understanding the cell's functional
704 organization. *Nature reviews. Genetics* **5**, 101-113 (2004).
- 705 30. M. R. Boyett, H. Honjo, I. Kodama, The sinoatrial node, a heterogeneous pacemaker
706 structure. *Cardiovascular research* **47**, 658-687 (2000).
- 707 31. H. Musa *et al.*, Heterogeneous expression of Ca(2+) handling proteins in rabbit sinoatrial
708 node. *The journal of histochemistry and cytochemistry : official journal of the*
709 *Histochemistry Society* **50**, 311-324 (2002).
- 710 32. M. B. Elowitz, A. J. Levine, E. D. Siggia, P. S. Swain, Stochastic gene expression in a
711 single cell. *Science* **297**, 1183-1186 (2002).
- 712 33. G. Gut, M. D. Herrmann, L. Pelkmans, Multiplexed protein maps link subcellular
713 organization to cellular states. *Science* **361** (2018).
- 714 34. A. Raj, A. van Oudenaarden, Nature, nurture, or chance: stochastic gene expression and
715 its consequences. *Cell* **135**, 216-226 (2008).
- 716 35. B. Cho *et al.*, Single-cell transcriptome maps of myeloid blood cell lineages in
717 *Drosophila*. *Nature communications* **11**, 4483 (2020).
- 718 36. B. Hudry *et al.*, Sex Differences in Intestinal Carbohydrate Metabolism Promote Food
719 Intake and Sperm Maturation. *Cell* **178**, 901-918 e916 (2019).

- 720 37. P. Mehta, T. Gregor, Approaching the molecular origins of collective dynamics in
721 oscillating cell populations. *Current opinion in genetics & development* **20**, 574-580
722 (2010).
- 723 38. P. S. Chen *et al.*, The initiation of the heart beat. *Circulation journal : official journal of*
724 *the Japanese Circulation Society* **74**, 221-225 (2010).
- 725 39. C. Liu, D. R. Weaver, S. H. Strogatz, S. M. Reppert, Cellular construction of a circadian
726 clock: period determination in the suprachiasmatic nuclei. *Cell* **91**, 855-860 (1997).
- 727 40. A. G. Siapas, E. V. Lubenov, M. A. Wilson, Prefrontal phase locking to hippocampal
728 theta oscillations. *Neuron* **46**, 141-151 (2005).
- 729 41. T. L. To, M. A. Henson, E. D. Herzog, F. J. Doyle, 3rd, A molecular model for
730 intercellular synchronization in the mammalian circadian clock. *Biophysical journal* **92**,
731 3792-3803 (2007).
- 732 42. E. Ullner, J. Buceta, A. Diez-Noguera, J. Garcia-Ojalvo, Noise-induced coherence in
733 multicellular circadian clocks. *Biophysical journal* **96**, 3573-3581 (2009).
- 734 43. E. Ullner, A. Zaikin, E. I. Volkov, J. Garcia-Ojalvo, Multistability and clustering in a
735 population of synthetic genetic oscillators via phase-repulsive cell-to-cell
736 communication. *Physical review letters* **99**, 148103 (2007).
- 737 44. L. Valon *et al.*, Robustness of epithelial sealing is an emerging property of local ERK
738 feedback driven by cell elimination. *Developmental cell* **56**, 1700-1711 e1708 (2021).
- 739 45. K. W. Pond *et al.*, Live-cell imaging in human colonic monolayers reveals ERK waves
740 limit the stem cell compartment to maintain epithelial homeostasis. *eLife* **11** (2022).
- 741 46. J. Schindelin *et al.*, Fiji: an open-source platform for biological-image analysis. *Nature*
742 *methods* **9**, 676-682 (2012).
- 743